JMEPEG (2019) 28:633–640
https://doi.org/10.1007/s11665-018-3614-1


1059-9495/$19.00

# Selective Reinforcement of Aerospace Structures Using Ultrasonic Additive Manufacturing

*Adam Hehr, Justin Wenning, Mark Norfolk, John Sheridan, John.A. Newman, and Marcia Domack*

*(Submitted March 21, 2018; in revised form June 25, 2018; published online August 29, 2018)*

**The combination of ultrasonic additive manufacturing (UAM) and metal matrix composite (MMC) materials enables novel and unique structures for the aerospace industry. This paper discusses tensile testing and modeling of MMC composites made with UAM for the first time. Composites built with 20, 34, and 45% MMC exhibited strengths near 430, 550, and 650 MPa, respectively. Complementary microscopy and CT scans are used to inform the modeling and testing effort. Modeling and testing show close agreement. Lastly, a non-standardized fatigue specimen is fabricated and tested to failure. The specimen began to crack near 500 k cycles and was resistant to failure (> 20 M cycles). On the other hand, a reference unreinforced specimen began to crack near 100 k cycles and failed near 180 k cycles.**

**Keywords** additive manufacturing, aerospace, aluminum, dynamic mechanical, metal matrix composite, static mechanical, structural ceramics

## 1. Introduction

### 1.1 Motivation

Today's energy and performance requirements are pushing for lighter, stronger, and faster aerospace vehicles. Economic considerations are also driving the need for low cost manufacturing options and efficient use of materials. To meet these demands, researchers have been developing new aluminum composite materials and designs.

Selective reinforcement or functionally graded materials use in structures is an approach that has been gaining attention regarding weight reduction and cost savings. Selective reinforcement works by putting strong, stiff, and potentially heavy material where needed and using lighter less stiff materials in areas of least concern. For example, Bucci (Ref 1) demonstrated a 25% weight reduction and a 25% fatigue life increase in an airframe structure using commercially available fiber metal laminates and glue joints. Farley glued or soldered selective reinforcement materials to aluminum structures to enhance the buckling load in panels by 68% (Ref 2), increased the fatigue and crack propagation resistance in aluminum alloys (Ref 3), and reduced stresses around holes in airframe structures (Ref 4). More recent MetPreg studies by Bird et al. (Ref 5) showed a 12% bending stiffness improvement in an aluminum structure when using diffusion bonding over glue.

Because selective reinforcement is limited in its application and design influence, Jutte et al. (Ref 6) proposed the concept of utilizing complex design and selective reinforcement together to meet performance goals. Jutte and team explored this concept computationally and proposed the use of a 3D printing technology for fabrication. However, no specific 3D printing technology was identified. Ultrasonic additive manufacturing (UAM) has the attributes to meet the requirements defined by Jutte and team.

The combination of UAM and metal matrix composite (MMC) materials enable the possibility for complex 3D printed designs with selective reinforcement and material grading. Because UAM works by layering materials together through ultrasonic metal welding, MMC's in laminate or rod form can be incorporated throughout the structure for tailored properties. UAM does not have atmospheric requirements, so large structures can also be fabricated (near 1.8 m × 1.8 m × 1 m). Also, the subtractive stage of UAM can be used to introduce complex features into the part. The idea of combining UAM and MMC laminates was initially explored by Stucker et al. (Ref 7, 8) through qualitative weld evaluations. Obielodan and Stucker (Ref 9, 10) then studied complex structure testing and found that added MMC's to an aluminum structure demonstrated higher failure loads and strain energy than a homogenous aluminum structure. No standardized testing of MMC samples was carried out to inform this complex structure testing, so design and analysis was somewhat limited.

The goals of this study are to (1) evaluate the tensile properties of UAM MMC composites samples built with varying volume fractions of MMC reinforcement, and (2) to demonstrate the use of MMC's in UAM structures. To date, this level of study has not been carried out to quantify the benefit of MetPreg using standardized mechanical testing. Rule-of-mixtures modeling is utilized to rationalize the composite behavior observed during testing. Complementary microscopy and CT scans are then utilized to inform this modeling effort. Lastly, fatigue testing is carried out on a structure reinforced with MMC's. This structure demonstrated an order of magnitude improvement in life relative to an unreinforced specimen.

### 1.2 Metal Matrix Composite Laminates

The MMC laminate used in this study, called MetPreg®, is manufactured by Touchstone Research Laboratory. MetPreg is

This article is an invited paper selected from presentations at the symposium "Additive Manufacturing of Composites and Complex Materials II," held during MS&T'17, October 8–12, 2017, in Pittsburgh, PA, and has been expanded from the original presentation.

**Adam Hehr, Justin Wenning,** and **Mark Norfolk**, Fabrisonic LLC, Columbus, OH 43221; **John Sheridan**, Sheridan Solutions LLC, Saline, MI 48176; **John. A. Newman** and **Marcia Domack**, NASA Langley Research Center, Hampton, VA 23681. Contact e-mail: ahehr@fabrisonic.com.

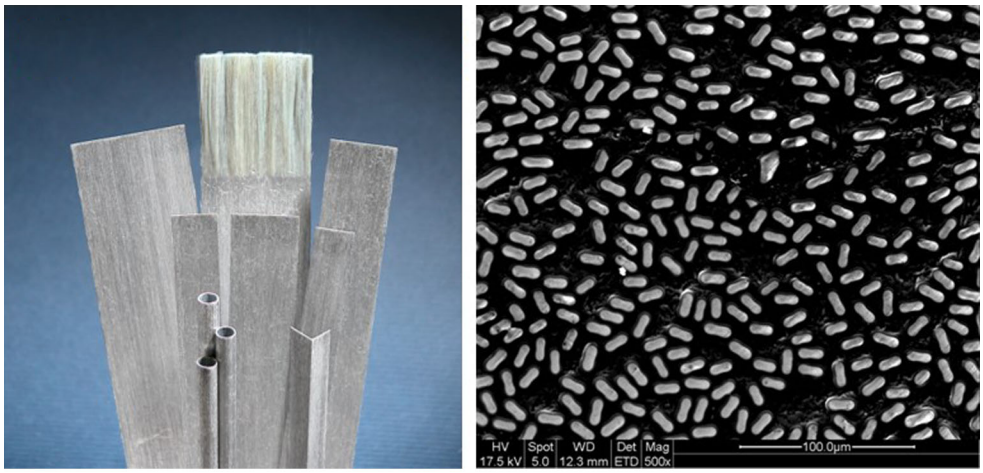


**Fig. 1** Commercial MetPreg: (a) various forms of MetPreg, image courtesy of Touchstone; (b) scanning electron microscope image of MetPreg displaying alumina fibers in an aluminum matrix

**Table 1 Typical MetPreg properties**

| Property | Value |
|---|---|
| Fiber volume fraction | 0.50 |
| Density, lb/in$^3$, g/cm$^3$ | 0.119 (3.30) |
| Maximum use temperature, °F, °C | 1000 (538) |
| 0° Tensile strength at RT, ksi, MPa | 210 (1448) |
| 0° Tensile modulus at RT, Msi, GPa | 33 (228) |
| 0° Compressive strength at RT, ksi, MPa | 500 (3447) |
| Elongation, % | 0.68 |
| Thermal expansion, in/in-°F, m/m-K | 4 (7) |
| Thermal conductivity, BTU/h-ft-°F (W/m-K) | 67 (116) |
| Electrical resistivity, Ω-nm | 50 |
| Shelf life at RT, months | Infinite |
| Volatile content by weight, % | 0 |

composed of commercial, continuous Nextel 610 alumina (aluminum oxide) fibers and a matrix of pure aluminum to create a unidirectional MMC. As described by Deve and McCullough (Ref 11), the soft aluminum matrix creates global load sharing behavior with the alumina, which in turn produces very high failure loads. Irick and Gordon (Ref 12) describe the manufacturing process of MetPreg in detail. Figure 1 summarizes frequent material forms of MetPreg, e.g., strip and tube and how the alumina is dispersed in aluminum. Commonly used MetPreg properties are shown in Table 1.

### *1.3 Ultrasonic Additive Manufacturing*

Invented by White (Ref 13), ultrasonic additive manufacturing (UAM) is a 3D metal printing technology that uses ultrasonic vibration energy to weld similar and dissimilar metal tapes together one layer at a time. The process operates near room temperature and the bonding mechanism does not rely on melting for joining. Instead, the ultrasonic vibrations of the process fracture surface oxides and bring metallic lattices intimately close, which in turn creates a metal-to-metal bond. Recently, the UAM weld tooling and process power limit was enhanced by Graff et al. (Ref 14) to join harder and stiffer metals, so-called high power UAM. High power UAM uses two 4.5 kW transducers operating in a push–pull configuration to create a 9 kW system. Earlier UAM systems used a single transducer with a power level of either 1.5 or 3 kW. In conjunction with the additive stage, periodic computer numerical control (CNC) machining operations are used interchangeably to introduce internal features and to finalize geometry of the printed part. Both large and small features can be accomplished with both high accuracy and smooth surface finish. No special atmospheric requirements exist for UAM, so the build envelope is flexible and bound only by the envelope of the CNC machine. A commercial UAM system and its tooling are shown in Fig. 2. The weld tooling is comprised of two high power ultrasonic transducers attached to an ultrasonic horn, see Fig. 2(b). The transducers excite the horn in a longitudinal scrubbing mode of vibration while the horn rotates along the weld surface. A down force is applied in tandem to the scrubbing motion to facilitate joining. This down force, scrubbing motion, and rolling speed are all controlled by the user at the onset of the process.

The solid-state, or no melting, nature of UAM enables bonding of aluminum alloys and joining of dissimilar metals because solidification and high-temperature chemistry is avoided and minimized, respectively. Sietins (Ref 15) showed that the diffusion between aluminum and copper is highly localized to the interface region, approximately 400 nm in thickness. Metals which have been joined to themselves and other metals include aluminum alloys (1xxx, 2xxx, 3xxx, 5xxx, 6xxx, 7xxx), coppers, stainless and 4xxx steels, and some titanium alloys. The combination of additive manufacturing, dissimilar metal joining, and subtractive operations of UAM enable fabrication of unique metal parts that are not possible with standard subtractive processes or fusion-based 3D printing, i.e., powder or filament processes. Welding and incorporating MMC's into components via UAM is one such example since melting between the fiber and metal matrix is avoided. In the component shown in Fig. 3, UAM enables localized and strategic MetPreg placement with robust metallic bonds. Added cooling channels along the top edge, not possible without 3D printing, further enhance operating limits.

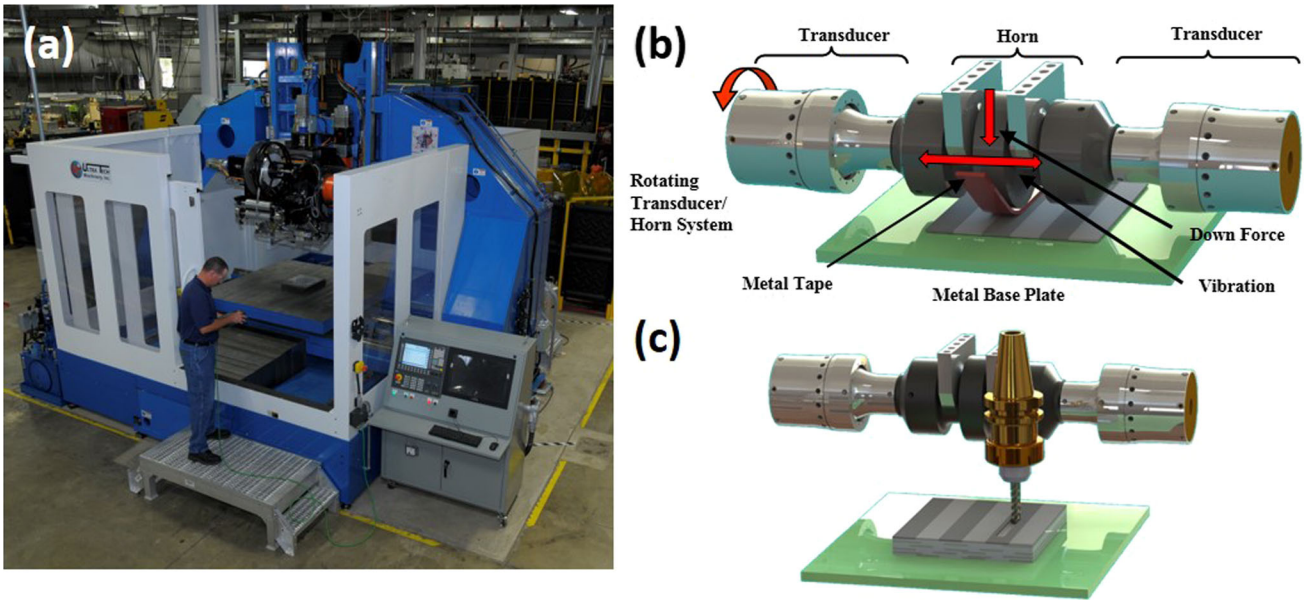


**Fig. 2** UAM process: (a) Fabrisonic SonicLayer™ 7200; (b) additive or ultrasonic welding stage of process; (c) subtractive or machining stage of process. The build envelope of the Fabrisonic SonicLayer™ 7200 is 1.8 × 1.8 × 1 m. Reprinted with permission

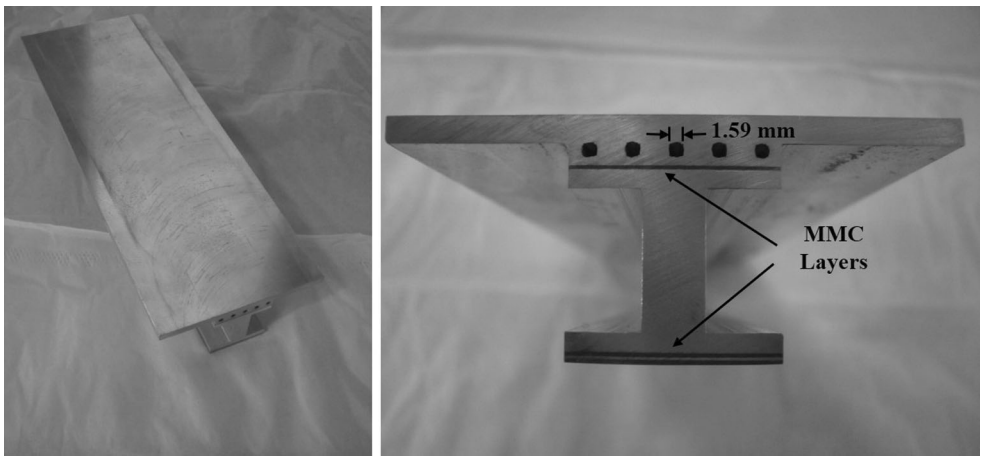


**Fig. 3** Rib fabricated with UAM using MMC's for enhanced stiffness and internal cooling channels for heat removal

## 2. Tensile Properties of Composites

### 2.1 Manufacturing

MetPreg material was provided by Touchstone. The provided MetPreg for sample manufacturing is 0.33 mm in thickness and 12.7 mm wide. The width of the welder is near 25.4 mm wide, so two of these MetPreg strips were run side-by-side simultaneously to make up the width difference during welding. A thin 0.05 mm sheet of aluminum 1100-H18 was used beneath layers of MetPreg during welding to enhance bonding. Aluminum 6061 foil in the H18* condition was used for welding between layers of MetPreg. Initial foil thickness is near 0.15 mm and the width is 25.4 mm. Figure 4 explains the build procedure for fabricating composites. The welding parameters used for construction are summarized in Table 2.

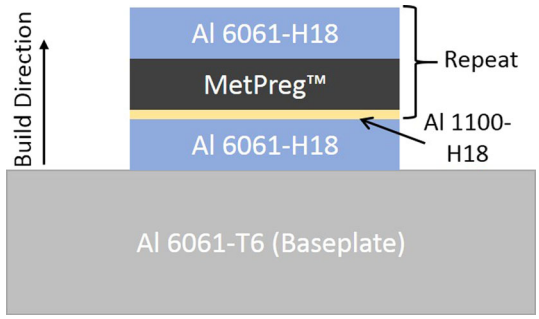


**Fig. 4** Representative build procedure for fabricating composites. The outlined section was repeated and adjusted to vary the volume percentage of MetPreg for the samples

*The foil is produced by cold rolling annealed 6061 billet to the final thickness (H18 condition).

Samples were made with one, two, and four layers of MetPreg in them using a consistent symmetric build pattern. Multiple layers of Al 6061-H18 were utilized between MetPreg layers to adjust the MetPreg volume fraction for a given sample. After welding, water jet cutting was used to cut tensile samples out following geometry specification given in ASTM D3552 (Ref 16). Samples were then machined down to final dimension by milling and removing the Al 6061-T6 baseplate in a vise using subtractive machining in the UAM machine.

An optical microscope image of an as-built composite sample with two layers of MetPreg is shown in Fig. 5. An abutting MetPreg joint is clearly seen in the top layer and not clearly seen in the bottom layer. An abutting joint is seen because two MetPreg strips are welded side by side, as discussed earlier. The bottom layer joint is not easily observed because the MetPreg tapes exhibited adequate overlap, whereas this did not occur on the top. Nonetheless, this joint is not a concern here due to its orientation with respect to the testing direction. Little to no porosity is observed in the sample.

**Table 2 Welding parameters used for composite fabrication**

| | MetPreg + Al 1100-H18 | Al 6061-H18 |
|---|---|---|
| Rolling travel speed, m/min | 3.81 | 4.45 |
| Down force, N | 4000 | 4000 |
| Peak-peak vibration, $\mu$m | 43.3 | 33 |
| Baseplate pre-heat, °C | 82.2 | 82.2 |

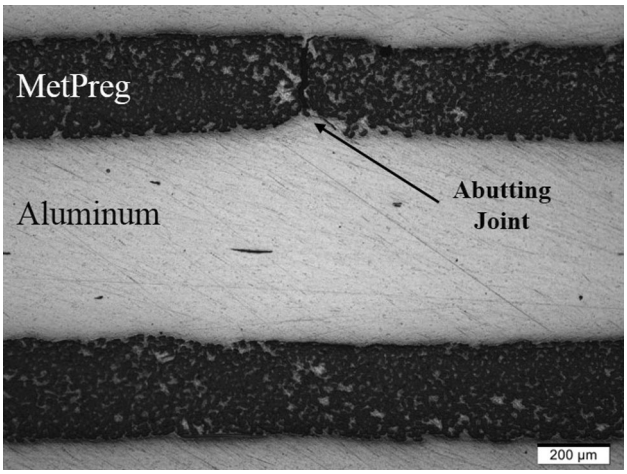


**Fig. 5** Optical microscope image of MetPreg composite. The abutting MetPreg joint is clearly visible for the top layer of MetPreg and not clearly visible for the bottom layer

### 2.2 Testing

Tensile testing was carried out following ASTM D3552. Testing was carried out at the Edison Welding Institute and Touchstone simultaneously to confirm composite performance independent of test machine and operator. Combined results from testing are summarized in Table 3. The volume fraction of MetPreg was estimated by measuring the total thickness of the composite and subtracting the total measured MetPreg thickness via optical microscopy.

A stress–strain summary of the composites is shown in Fig. 6. The stress–strain curves of welded Al 6061-H18 and MetPreg are also plotted for comparison purposes. The composite strength is bound by the two constituents of the composite, i.e., 6061-H18 and MetPreg. The failure strain of the composite is also similar to that of the MetPreg. Figure 7 is a correlation between the MetPreg volume fraction and ultimate tensile strength for each material in Fig. 6. The trend between MetPreg volume fraction and strength is linear, which implies that the composite follows rule-of-mixture behavior.

Figure 8 describes the failure modes observed in the MetPreg composites. In general, the composites demonstrate brittle failure because little to no necking or ductility was observed, see Fig. 8(a). Figure 8(b) indicates that this brittle failure is driven by the MetPreg because the MetPreg itself exhibits brittle failure. The high load sharing of the MetPreg in the composite is the reason for this failure behavior. On the other hand, the aluminum weld metal is comparatively more

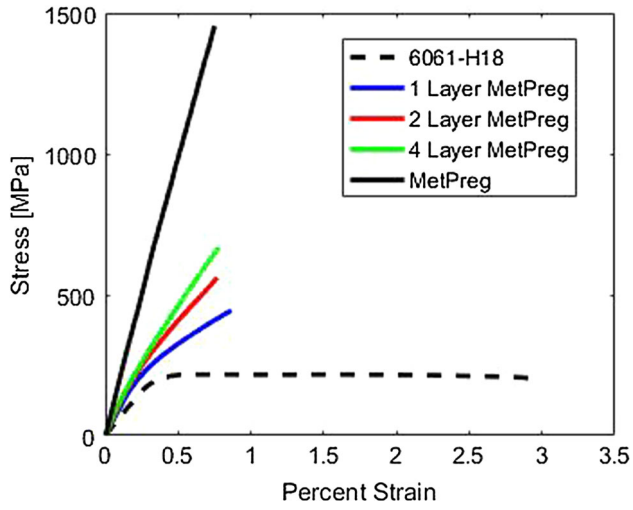


**Fig. 6** Stress–strain comparison of composite constituents and composites themselves. The composites fail near the failure strain of the MetPreg. More MetPreg creates a stronger composite. Data provided by Touchstone

**Table 3 Comparative evaluation of Edison Welding Institute (EWI) and Touchstone testing results for MetPreg samples**

| MetPreg layers | 1 | 2 | 4 |
|---|---|---|---|
| Volume percent MetPreg, % | 20 | 34 | 45 |
| Measured strength, MPa | 434.8 | 555.5 | 664.3 |
| Measured strength standard deviation, MPa | 13.3 | 22.9 | 25.9 |
| No. tested samples | 9 | 8 | 11 |

The results show close correlation

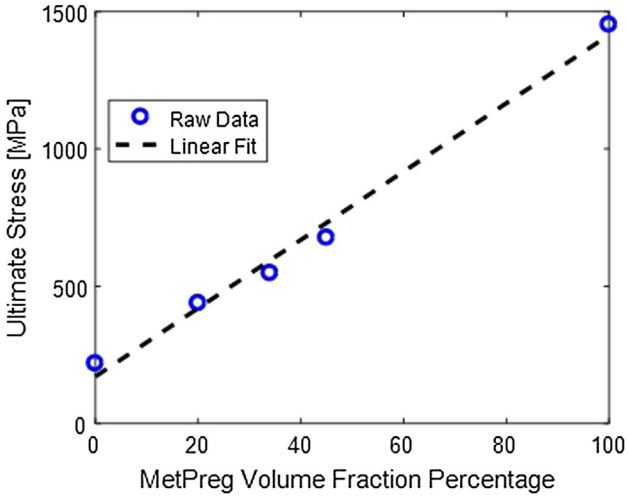


**Fig. 7** Correlation between strength and MetPreg volume fraction. The linear trend implies rule-of-mixture behavior with the composite. The $R^2$ value is 0.99. Data provided by Touchstone

ductile, and localized areas of ductility are observed at the failure surface.

## 3. Modeling Performance

### 3.1 Rule of Mixtures

Rule-of-mixtures were utilized to model the composite because of the linear correlation between ultimate tensile strength and MetPreg volume fraction in Fig. 7. As explained by Agarwal et al. (Ref 17), the rule-of-mixture principle could be applied to both ultimate strength and modulus of elasticity because of the brittle failure mode of the composite. The expressions for composite strength ($\sigma$) and modulus of elasticity ($E$) in the loading direction can be written as,

$$\sigma_{\text{comp}} = \sigma_{\text{MMC}} V_{\text{MMC}} + (\sigma_{\text{Al6061}})_{\varepsilon_f^*} V_{\text{Al6061}} + (\sigma_{\text{Al1100}})_{\varepsilon_f^*} V_{\text{Al1100}}, \quad \text{(Eq 1)}$$

$$\text{and} \quad E_{\text{comp}} = E_{\text{MMC}} V_{\text{MMC}} + E_{\text{Al6061}} V_{\text{Al6061}} + E_{\text{Al1100}} V_{\text{Al1100}}. \quad \text{(Eq 2)}$$

where $V$ is the volume percent of each constituent in the composite. The analysis includes a small estimated volume fraction ($\sim$ 5%) of Al 1100-H18, assumed to be 152 MPa in strength.** As mentioned previously, the MetPreg volume fraction was measured using microscopy. Hence, the Al 6061 volume fraction was estimated by subtracting the measured MetPreg volume fraction and estimated Al 1100 volume fraction from the total. This analysis uses measured ultimate strength at the failure strain of the composite ($\varepsilon_f^*$) for the Al 6061-H18 and MetPreg. The modulus calculation uses measured MetPreg performance and handbook values for Al 6061 and Al 1100. The failure strain of the MetPreg and composite are assumed to be equal for this strength calculation analysis due to their similar values in Fig. 6. Table 4 summarizes the analysis for the composites.

**Quantity from matweb.com.

The theoretical and measured results demonstrate good correlation. The model deviation is near or above 10% for the strength and less than 5% for the modulus of elasticity. It is interesting to note that the model deviation is generally greater than zero, which implies that this initial model overpredicts performance.

### 3.2 Incorporating Broken Fibers

The rule-of-mixtures analysis in Table 4 overpredicts performance, which implies that one of the constituents is not retaining its strength after welding. MetPreg is an obvious suspect because the UAM tooling contacts it directly during welding. The weld tooling contact is known to damage fibers locally on the surface, yet this damage zone has not previously been evaluated. During this research, CT-scanning and optical microscopy were utilized to assess and quantify the fiber breakage in a small number of representative samples, see Fig. 9. It is assumed that the observed trends in these samples can be extrapolated to all other samples in this study.

The imaging reveals that the fiber breakage is near 10% of the MetPreg layer thickness. This 10% fiber breakage was quantified by measuring the thickness of broken fibers in the CT and optical image, see Fig. 9. The broken fibers cause the MetPreg to underperform. To incorporate the influence of the broken fibers into the model for strength and modulus of elasticity, the MetPreg volume fraction can be adjusted by adding a broken volume fraction term ($V_{\text{broken}}$),

$$\sigma^*_{\text{comp}} = \sigma_{\text{MMC}}(V_{\text{MMC}} - V_{\text{broken}}) + (\sigma_{\text{Al6061}})_{\varepsilon_f^*} V_{\text{Al6061}} + (\sigma_{\text{Al1100}})_{\varepsilon_f^*}(V_{\text{Al1100}} + V_{\text{broken}}), \quad \text{(Eq 3)}$$

$$\text{and} \quad E^*_{\text{comp}} = E_{\text{MMC}}(V_{\text{MMC}} - V_{\text{broken}}) + E_{\text{Al6061}} V_{\text{Al6061}} + E_{\text{Al1100}}(V_{\text{Al1100}} + V_{\text{broken}}). \quad \text{(Eq 4)}$$

The broken volume fraction is removed from the MetPreg total and added to the Al 1100 constituent due to the matrix metal of MetPreg being Al 1100 (assuming broken fibers add no reinforcement). Table 5 summarizes the results with the adjusted fiber breakage volume. With this adjustment, the model deviation between theory and measurement decreases to near 5% and oscillates around zero.

## 4. Fatigue Testing

Using the knowledge gained from mechanical testing and analysis of UAM MMC composites, a fatigue specimen was built with MetPreg in high stress regions for reinforcement purposes, see Fig. 10(a). This specimen is near 10 cm in width, 50 cm in length, and 1 cm in thickness. NASA LaRC's Digital Twin Project developed this fatigue specimen such that similar stress concentrations were experienced at multiple locations (giving multiple sites where crack initiation is likely) while preserving some of the features of truss-braced-wing structural components (Ref 18). Failure prediction is confused because the bolt hole and notch stress risers have nearly identical failure loads. NASA LaRC tested an unreinforced reference sample prior to the development of this sample as a benchmark.

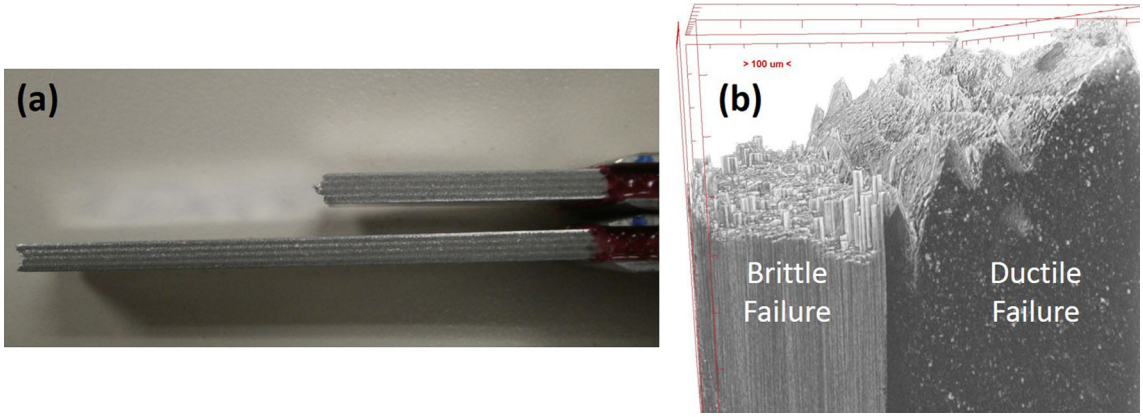


**Fig. 8** Failed MetPreg composite sample: (a) 4-layer MetPreg composite that fails in brittle mode; (b) CT-Scan of composite failure surface showing brittle failure in the MetPreg and ductile failure in the welded aluminum

**Table 4 Rule-of-mixtures analysis for composites using measured Al 6061-H18 and MetPreg strength**

| MetPreg volume percent, % | 0 | 20 | 34 | 45 | 100 |
|---|---|---|---|---|---|
| Theoretical strength, MPa | N/A | 461.3 | 637.3 | 766.9 | N/A |
| Measured strength, MPa | 217.9 | 434.8 | 555.5 | 664.3 | 1452.7 |
| Measured strength standard deviation, MPa | 1.2 | 13.3 | 22.9 | 25.9 | 176.5 |
| Strength percent difference, % | N/A | 6.1 | 14.7 | 15.4 | N/A |
| Theoretical modulus, MPa | 68.9 | 95.7 | 115.1 | 129.3 | N/A |
| Measured modulus, GPa | N/A | 94.0 | 110.4 | 130.4 | 203.7 |
| Measured modulus standard deviation, GPa | N/A | 1.7 | 2.2 | 5.7 | 13.6 |
| Modulus percent difference, % | N/A | 1.8 | 4.1 | − 0.8 | N/A |

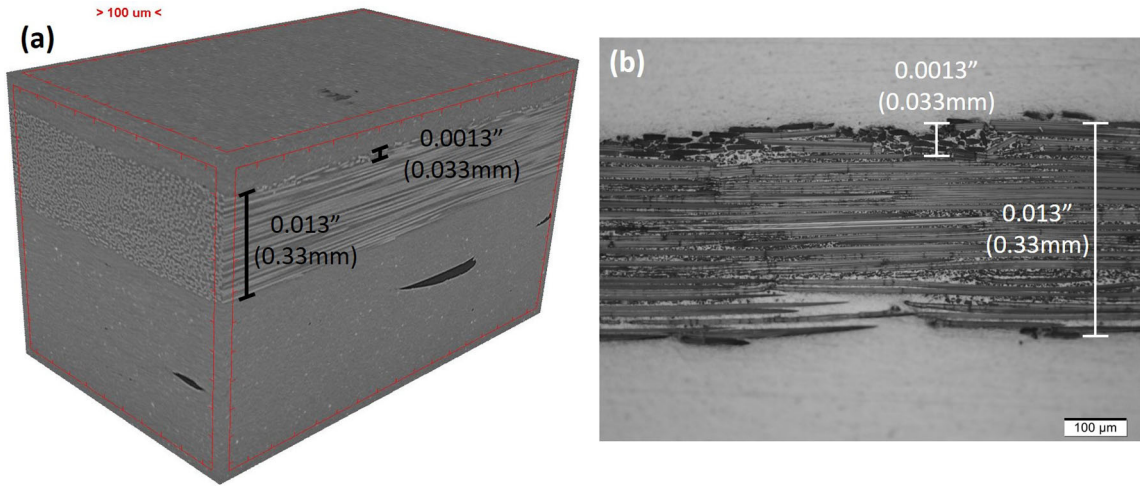


**Fig. 9** Broken fiber analysis in MetPreg: (a) CT-scan showing broken fibers near top of layer; (b) optical image taken with fibers running in-plane showing corroborating information shown in (a). Nearly 10% of the fibers appear to be broken in the images

To design the reinforced fatigue sample, 3D elastic finite element modeling (FEM) was used to guide placement of the MetPreg within the sample. Static analysis within ANSYS Workbench 12.0 was used to describe the physics of the specimen. Solid, contact, and surface elements were utilized and generated using the default mesh generator tool with Workbench. All contact surfaces were assumed to be fixed. MetPreg was modeled as a customized anisotropic material using measured properties of the welded material, i.e., fiber breakage was considered. The other material properties in the material matrix were assumed to be Al 1100-H18 handbook values. The output of the FEM to make design refinement decisions was the peak stress near the bolt holes and notches within the Al 6061. MetPreg was added to the sample around the bolt holes and notches such that the von Mises peak stress in the Al 6061 would be at least 20% lower in magnitude. The location and quantity of MetPreg at a given location were iterated upon to arrive at the final design. The final design of the sample uses two internal layers of MetPreg to manage stress from the notch while two external layers are added to manage the stress from the bolt holes. The MetPreg used for this sample design is near 25 mm in width and 0.5 mm in thickness.

**Table 5 Rule-of-mixtures analysis with broken fibers in MetPreg considered. The MetPreg volume fraction reduces by nearly 10% in the model**

| MetPreg volume percent, % | 0 | 20 | 34 | 45 | 100 |
|---|---|---|---|---|---|
| Theoretical strength, MPa | N/A | 435.4 | 592.7 | 708.5 | N/A |
| Measured strength, MPa | 217.9 | 434.8 | 555.5 | 664.3 | 1452.7 |
| Measured strength standard deviation, MPa | 1.2 | 13.3 | 22.9 | 25.9 | 176.5 |
| Strength percent difference, % | N/A | 0.15 | 6.3 | 6.3 | N/A |
| Theoretical modulus, MPa | 68.9 | 93.0 | 110.5 | 123.3 | N/A |
| Measured modulus, GPa | N/A | 94.0 | 110.4 | 130.4 | 203.7 |
| Measured modulus standard deviation, GPa | N/A | 1.7 | 2.2 | 5.7 | 13.6 |
| Modulus percent difference, % | N/A | − 1.0 | 0.1 | − 5.7 | N/A |

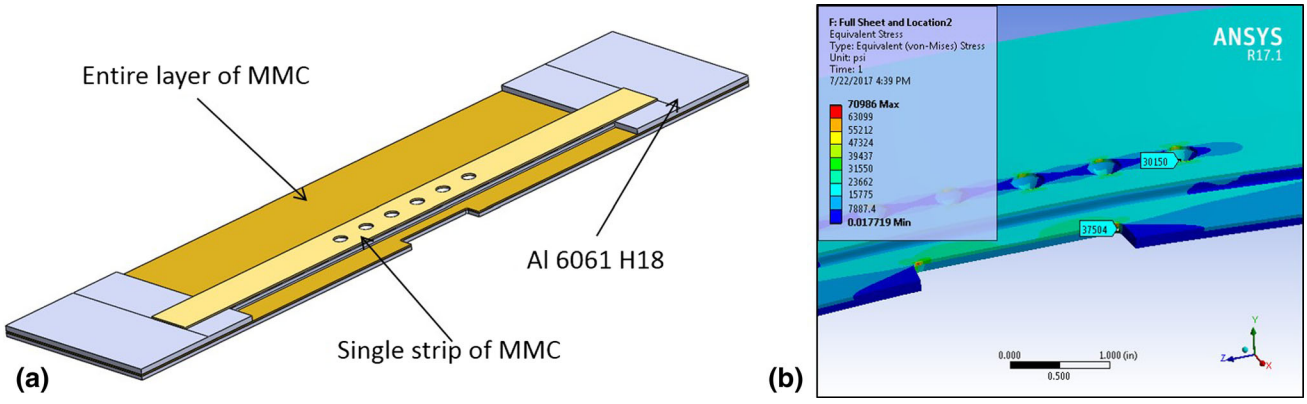


**Fig. 10** Fatigue specimen design and analysis: (a) atypical fatigue specimen with MMC reinforcement around stress risers. MMC was added in the body of the part to manage stress from the notches and added to the top of the part around the bolt hole stress risers; (b) linear elastic FEM modeling in ANSYS was used to guide the design of the fatigue part

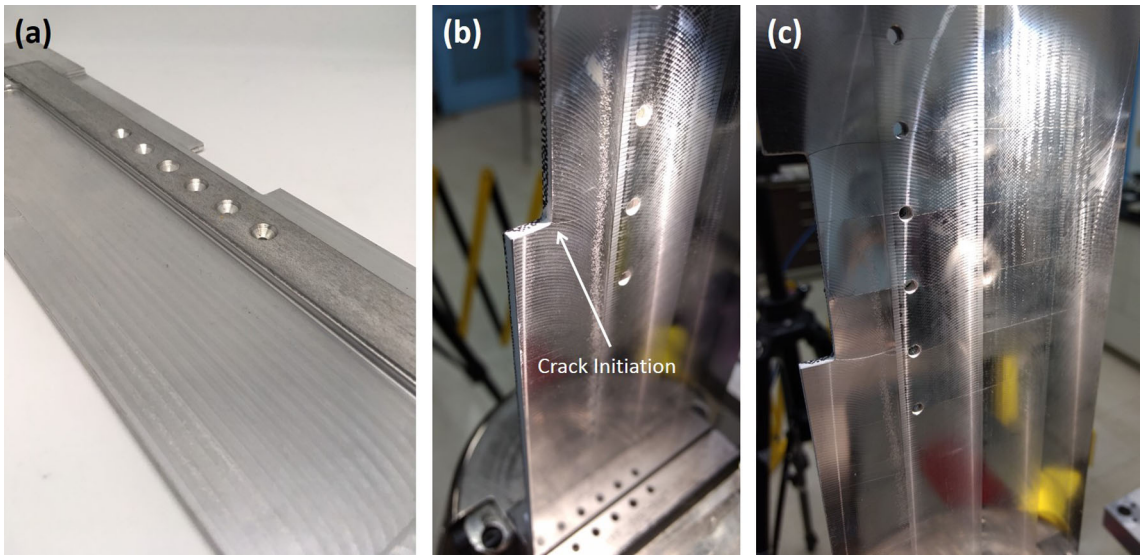


**Fig. 11** Fatigue testing: (a) fabricated part; (b) crack initiation near 1 M cycles; (c) crack evolution near 16 M cycles. The life of the part demonstrated near an order of magnitude enhancement in crack initiation and total life

To manufacture an entire layer of MMC material, the strips were staggered side by side with an interference fit for the abutting joint. The Al 6061-H18 material was 3D printed using sheet form. Similar to the MetPreg layers, the Al 6061 material was 3D printed by translating the UAM tooling from side to side for scale-up. All cutting operations were carried out using the subtractive stage of the UAM process. The final part is shown in Fig. 11(a).

Fatigue testing took place at NASA LaRC using a 44.5 kN servo-hydraulic MTS 810 test frame with hydraulic grips near

**Table 6 Comparison of fatigue sample performance for unreinforced and reinforced specimens**

| | Crack initiation cycle no. | Failure cycle no. |
|---|---|---|
| Unreinforced specimen | 110 k | 177 k |
| Reinforced specimen | 497 k | > 20 M |

10 cm in width to constrain the sample. The sample was constrained within the grips using a pressure of 20 MPa, a value found by experience to prevent aluminum sample slip and to avoid crushing the sample. The grip load is assumed to not influence the test since it is sufficiently far from the area of concern, i.e., Saint-venant principle. The sample was axially loaded by cycling between 3 and 30 kN tensile loads at a frequency of 10 Hz. The specimen was inspected every 50-100 k cycles until the first crack was observed. The first crack was observed near 500 k cycles, see Fig. 11(b). This crack initiation was near 3 times greater than the non-reinforced benchmark. The sample was then cycled in larger cycle increments (200-500 k cycles) such that damage could be progressed within the sample. It was found that the sample was resistant to failure at high cycle counts. Figure 11(c) shows the sample at 16 M cycles (near 100 times higher life than unreinforced specimen). Cracking is observed at all of the stress concentration areas in the sample. The results from the fatigue test are summarized in Table 6 along with the unreinforced reference specimen.

Due to the specimen being resistant to failure, cycling was ceased at 20 M cycles (120 times higher life than unreinforced specimen). The sample was then axially pulled apart such that the failure interfaces could be inspected to better understand the failure modes and how damage progressed within the sample. The team plans to publish later on this fractography analysis.

## 5. Summary and Future Work

This study demonstrated fabrication of aluminum-based MMCs unidirectionally reinforced with MetPreg. Metallurgical analysis confirmed consolidation between aluminum foil and MetPreg layers with little to no porosity. Composites built with 20, 34, and 45% MetPreg exhibited strengths near 430, 550, and 650 MPa, respectively, as compared with 218 MPa for unreinforced 6061. The trend of strength with volume fraction of MetPreg followed rule-of-mixtures behavior; however, conventional analysis overpredicted strength levels. CT analysis confirmed that approximately 10% of the MetPreg fibers were damaged during consolidation. The rule-of-mixtures analysis was modified to account for the damaged fibers to predict tensile properties. Future work should examine processing modifications to reduce or eliminate fiber damage in order to maximize the performance attributes of the MetPreg. Lastly, a scaled-up component with selectively reinforced MMC was fatigue tested. The specimen began to crack near 500 k cycles and was resistant to failure (> 20 M cycles). On the other hand, a reference unreinforced specimen began to crack near 100 k cycles and failed near 180 k cycles.


## Acknowledgments

The authors would like to acknowledge financial support from NASA's SBIR Office, NNX16CL34C. The authors are grateful for the support of Dr. Jennifer Sietins, Army Research Labs, who provided the CT-scan analysis. Support from Brian Gordon at Touchstone is also appreciated.


## References


1. R. Bucci, Advanced Metallic & Hybrid Structural Concepts, *USAF Structural Integrity Program Conference*, San Antonio, TX, 2006
2. G.L. Farley, Selective Reinforcement to Enhance the Structural Performance of Metallic Compression Panels, *AIAA Structures, Structural Dynamics and Materials Conference*, Palm Springs, CA, 2004
3. G.L. Farley, J.A. Newman, and M.A. James, Selective Reinforcment to Improve Fracture Toughness and Fatigue Crack Growth Resistance in Metallic Structures, *AIAA Structures, Structural Dynamics and Materials Conference*, Palm Springs, CA, 2004
4. G.L. Farley and B.R. Seshadri, Performance Enhancement Using Selective Reinforcement for Metallic Single- and Multi-pin Loaded Holes, *AIAA Structures, Structural Dynamics and Materials Conference*, Austin, TX, 2005
5. R.K. Bird, J.A. Alexa, P.L. Messick, M.S. Domack, and J.A. Wagner, *Investigation of Methods for Selectively Reinforcing Aluminum and Aluminum-Lithium Materials*, NASA Langley Research Center, Hampton, VA, 2013
6. C.V. Jutte, B.K. Stanford, C.D. Wieseman, and J.B. Moore, *Aeroelastic Tailoring of the NASA Common Research Model via Novel Material and Structural Configurations*, AIAA SciTech Conference, National Harbor, MD, 2014
7. B. Stucker, J. Obielodan, A. Ceylan, and L. Murr, Multi-Material Bonding in Ultrasonic Consolidation, *Rapid Prototyp. J.*, 2010, **16**(3), p 180–188
8. G. Janaki Ram, C. Robinson, Y. Yang, and B. Stucker, Use of Ultrasonic Consolidation for Fabrication of Multi-Material Structures, *Rapid Prototyp. J.*, 2007, **13**(4), p 226–235
9. J. Obielodan and B. Stucker, *Dual-Material Minimum Weight Structures Fabrication Using Ultrasonic Consolidation*, Solid Freeform Fabrication Symposium, Austin, TX, 2010
10. J. Obielodan and B. Stucker, A fabrication Methodology for Dual-Material Engineering Structures Using Ultrasonic Additive Manufacturing, *Int. J. Adv. Manuf. Technol.*, 2014, **70**, p 277–284
11. H. Deve and C. McCullough, Continuous-Fiber Reinforced Al Composites: A New Generation, *JOM*, 1995, **47**(7), p 33–37
12. V. Irick and B. Gordon, MetPreg Metallic Prepregs for the Composites Industry, *SAMPE J.*, 2004, **40**(2), p 8–15
13. D. White, Ultrasonic Consolidation of Aluminum Tooling, *Adv. Mater. Process.*, 2003, **161**(1), p 64–65
14. K. Graff, M. Short, and M. Norfolk, *Very High Power Ultrasonic Additive Manufacturing (VHP UAM) for Advanced Materials*, Solid Freeform Fabrication Symposium, Austin, TX, 2010
15. J. Sietins, Exploring Diffusion of Ultrasonically Consolidated Aluminum and Copper Films Through Scanning and Transmission Electron Microscopy, Ph.D. thesis, University of Delaware, 2014
16. ASTM, *Standard Test Method for Tensile Properties of Fiber Reinforced Metal Matrix Composites*, 2016. https://www.astm.org/Standards/D3552.htm
17. B.D. Agarwal, L.J. Broutman, and K. Chandrashekhara, *Analysis and Performance of Fiber Composites*, Wiley, Hoboken, 2006
18. P. Leser, Probabilistic Prognostics and Health Managment for Fatigue-crical Components using High-Fidelity Models, Ph.D. thesis, North Carolina State University, 2017